A waveguide-integrated superconducting nanowire single-photon detector with a spot-size converter on a Si photonics platform

Hiroyuki Shibata[1], Tatsurou Hiraki[2,3] , Tai Tsuchizawa[2,3], Koji Yamada[2,3], Yasuhiro Tokura[4] and Sinji Matsuo[2,3]

[1] Department of Electrical and Electronic Engineering, Kitami Institute of Technology, 165 Koen-cho Kitami, Hokkaido 090-8507, Japan
[2] NTT Device Technology Laboratories, NTT Corporation, 3-1 Wakamiya, Atsugi-shi, Kanagawa, 243-0198, Japan
[3] NTT Nanophotonics Center, NTT Corporation, 3-1 Wakamiya, Atsugi-shi, Kanagawa, 243-0198, Japan
[4] NTT Basic Research Laboratories, NTT Corporation, 3-1 Wakamiya, Atsugi-shi, Kanagawa, 243-0198, Japan

E-mail: shibathr@mail.kitami-it.ac.jp

Abstract
We report a high system-detection-efficiency superconducting nanowire single-photon detector (SNSPD) with a spot-size converter (SSC) on a Si photonics platform. The NbN-SNSPD is evanescently coupled to the Si waveguide and connected to the optical fibre through the low-loss SSC comprising a Si inverse taper and large silica-based core. The fabricated SNSPD chip was assembled on a low-loss fibre-coupled module. The fibre-coupling loss of the module is remarkably small (1.9 dB/facet). The fabricated SNSPD module shows system detection efficiency of 32% with the dark count rate of 95 Hz and timing jitter of 75 ps. The measured system detection efficiency is over ten times larger than that of previous waveguide-integrated SNSPDs on the Si platform. The noise equivalent power (NEP) reaches 3.6×10^{-18} $WHz^{-1/2}$, and the figure of merit (FOM) reaches 1.9×10^{8}.

Keywords: SSPD, SNSPD, Si waveguide

1. Introduction

Quantum photonic technology is attracting attention for applications in computing and communications [1-5]. The technology is promising for the development of quantum computers which have a possibility of solving problems that are hard or even impossible to solve with a classical approach [1,2], and it has been used in experimental demonstrations of quantum key distribution secure communications [3-6]. In these systems, the key challenges are to realize a high-efficiency single-photon source, high-efficiency single-photon detectors, and low-loss and scalable photonic circuits. To meet these challenges, many researchers have focused on the mature infrared photonic-integrated-circuit (PIC) technology that is widely used in practical telecommunications systems. In particular, the silicon (Si) platform has emerged as the best solution for scalability and cost-effective manufacturing [7-10]. Past work using the platform includes demonstrations of high-efficiency correlated photon-pair generation with Si and waveguides [7,8], and the development of low-loss quantum photonic circuits on silica-on-silicon waveguides [9,10].

One of the difficult challenges with infrared Si PICs is how to construct a low-loss quantum photonic receiver. The optical loss in the system exponentially decreases the probability of multiple photon coincidence; therefore, reducing it is essential for scaling up to large quantum computing circuits. The key figure of merit of the receiver is system detection efficiency, which includes the on-chip detection efficiency of each single-photon detector and fibre-coupling efficiency. Although the traditional Si avalanche photodiode (APD) typically shows good performance in the visible wavelength regime, it cannot detect infrared photons. Therefore, an alternative device should be introduced on the Si platform, and a promising one is the superconducting nanowire (nanostrip) single-photon detector (SNSPD, SSPD) [11-15]. An SNSPD enables high detection efficiency of infrared photons with a low dark count rate and small jitter. In particular, a waveguide-integrated SNSPD is preferable because it can be evanescently coupled to a PIC with short length and provide high detection efficiency and high-speed operation. However, the system detection efficiencies of SNSPDs are still limited due to a large fibre-coupling loss, which is caused by the large difference in the mode field diameters between the fibre and nanowire waveguide. Although a grating coupler, used as a typical fibre-chip interface, can be easily fabricated with the conventional Si photonics process, the second-order Bragg diffraction and poor fabrication tolerance cause a large fibre coupling loss. In addition, the 3-dB bandwidth of a grating coupler is small (< ~50 nm) and thus has strong wavelength dependence [16]. As a result, previously reported system detection efficiencies, including the fibre coupling loss, are limited to several percent.

To overcome this critical issue, a spot-size converter (SSCs) is required for the fibre-chip interface [17-20]. The Si inverse taper of an SSC connects a Si nanowire waveguide to

the large core (i.e. silica-on-silicon) with a low loss. The mode field diameter of the large core almost matches that of the optical fibre. As a result, the fibre coupling loss of the system becomes small. This also enables butt coupling to the fibre, which results in coupling loss independent of the wavelength. While SSCs have such advantages, it is difficult to fabricate a large core without damaging the superconducting material. For example, silica-on-silicon waveguides [10] whose mode field diameter almost matches that of the fibre have typically been fabricated by flame hydrolysis deposition at temperatures over 1000 °C. However, such high temperatures cannot be acceptable for the superconducting materials.

To address these problems, we monolithically integrated a waveguide-integrated SNSPD and SSC on the Si photonics platform. The key technology is low temperature fabrication of a large silica-based core without thermal degradation of the superconducting materials. It can reduce the fibre coupling loss without causing degradation of the detection efficiency of the SNSPD. In addition, we also developed a fibre-coupled module for cryogenic operation of the SNSPD chip. With this module, we can avoid difficult fibre alignment in the cryostat and therefore prevent fibre misalignment. In following sections, we describe in details of the design, fabrication, and measured characteristics of the waveguide-integrated SNSPD with the SSC chip, assembled in the fibre-coupled module.

2. Design and fabrication

Figure 1 (a) ~ (c) show the fabrication procedure for the waveguide-integrated niobium nitride (NbN) SNSPD with the SSC on a Si platform. The SNSPD chip has 1-mm-long silica-based core, 300-μm-long Si taper, and 4.3-mm-long Si nanowire waveguide between the fibre-chip interface and SNSPD. First, we fabricated the NbN SNSPD on the silicon-on-insulator wafer, whose Si and buried-oxide thickness were 200 nm and 3 μm, respectively. The NbN film was deposited by magnetron sputtering [21] and patterned by electron-beam lithography and dry etching [Fig. 1 (a)]. The width and thickness of the NbN nanowire were

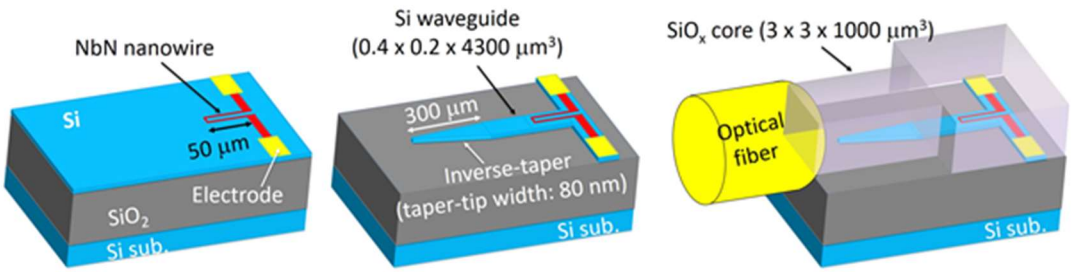

(a) (b) (c)

Figure 1. Fabrication procedure for the SNSPD with the SSC at (a) SNSPD, (b) Si waveguide, and (c) silica-base core formations.

60 and 7 nm, respectively. The coupling length between the NbN nanowire and Si waveguide was 50 μm. The electrode was formed by using titanium, gold, and chromium. Next, the Si waveguide was fabricated by using electron-beam lithography and dry etching [Fig. 1 (b)]. The core of the Si waveguide is 0.4 × 0.2 μm^2, and the taper-tip width and taper length of the SSC are 80 nm and 300 μm, respectively [19]. After that, the 3-μm^2 Si-rich silica-based core (SiO_x core) was formed by using the electron-cyclotron resonance (ECR) plasma enhanced chemical-vapor deposition (PE CVD) method at around 150 °C [Fig. 1 (c)], followed by the deposition of a 6-μm-thick SiO_2 overclad film. To match the mode field diameter of the SiO_x core to that of the high numerical aperture (NA) fibre (4.3 μm), the refractive indices of the core and clad film were set to 1.505 and 1.46, respectively. Finally, the electrical contact hole was formed by using the dry etching process. The key feature of the above procedure is the low temperature formation of the SiO_x core [18]. By changing the atomic composition of Si and O of the ECR plasma, it is possible to precisely control the refractive index of the SiO_x film from 1.46 to 1.7 at a temperature of less than 200 °C. Such a low temperature is beneficial for preventing thermal degradation of the SNSPD. The atomic composition of the core and clad film were $SiO_{1.7}$ and SiO_2, measured by the Rutherford backscattering spectrum [19].

(a)

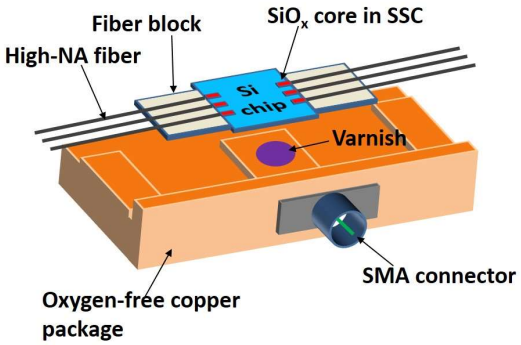

(b)

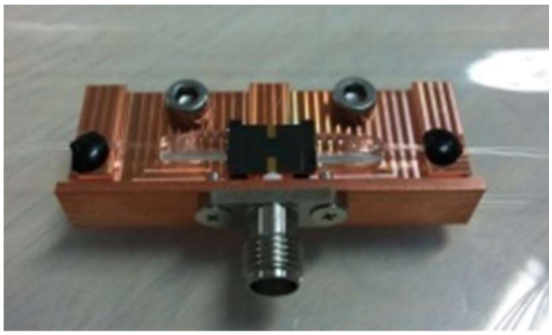

Figure 2. (a) Schematic of fibre-coupled module and (b) fabricated module.

After the fabrication, the wafer was diced and the chip facet was polished. Then the fabricated SNSPD chip was mounted on the fibre-coupled module, shown in Fig. 2(a) [22]. To obtain high thermal conductivity, we made the package out of oxygen-free cooper. In addition, we mounted the Si chip on the package with varnish. The result is that the chip and package have almost the same temperature as the cryostat stage. As the optical fibre, we used high NA fibre with a mode field diameter of 4.3 μm. It is attached to the SSCs at the facet of the Si chip with resin adhesive, which is suitable for ultralow temperatures (NTT Advanced

Tech. Co., custom made). This prevents misalignment at the fibre/chip interface under cryogenic conditions, which is beneficial for the system cost effectiveness because an expensive fibre positioner in the cryostat is not required [11]. The electrical signals can be obtained from SMA (SubMiniature version A) connectors attached to the outside of the module. The signal line of the SMA connectors was bonded to the electrode on the chip with Ag past. Figure 2(b) shows a photograph of the fabricated SNSPD module. The module size is 45 × 17 mm^2.

3. Device characteristics

3.1 Optical loss

First, we checked the optical loss of the Si waveguide and SSC. Before mounting the Si chip on the package, we measured the transmittance of the Si waveguide chip with the SSC on an optical stage at room temperature. The waveguide chip was fabricated with the SNSPD chip on the same wafer. As a reference, we also measured the loss of a typical Si waveguide chip, which was fabricated without integrating the SNSPD [22]. In the measurement, the light source was amplified spontaneous emission (ASE) in the transverse electric (TE) mode. The output power was normalized by the fibre-to-fibre transmission. Figure 3(a) shows the relationships between the transmittance and the length of the Si waveguide with the SSC at a wavelength of 1550 nm. We found the propagation loss to be 3.7 dB/cm and the coupling loss to be 0.9 dB/facet. Compared with the results for the reference Si waveguide (1.3 dB/cm), the propagation loss was slightly larger. This is presumably due to damage of the Si waveguide caused by the dry etching of the NbN. The damage can be reduced by preventing the over-etching to the Si waveguide. On the other hand, the fibre coupling losses are not different between the two types of the Si waveguides. Therefore, the loss of the inverse taper and SiO_x waveguide was not degraded by the NbN integration.

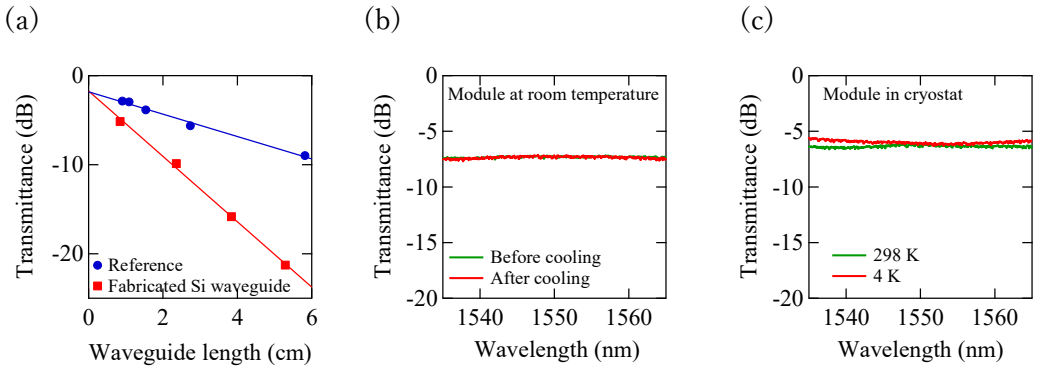

Figure 3. (a) Transmission of Si waveguide with SSC, and transmission spectrum of assembled Si waveguide chip (b) before and after cooling and (c) at room temperature and 4K.

Next, we checked the fibre coupling loss after assembly. We mounted the reference Si waveguide on the package and measured the transmission spectrum. We measured the transmittance of the 2.74-cm-long Si-waveguide module at room temperature by introducing ASE light into the module's input port. Figure 3(b) shows the measured results. By subtracting the propagation loss of the Si waveguide, the fibre-coupling loss of the module was estimated to be 1.9 dB/facet, which included the loss of the SSC (0.9 dB) and the loss of fibre/chip interface (1.0 dB). We also measured the propagation characteristics of the module at 4 K. Figure 3(c) shows the normalized transmission spectra in the cryostat. The results show no degradation of transmission characteristics at 4 K. The loss of the module is more than 10 dB lower than that of grating couplers at the entire C band [16]. After the cryogenic measurement, we removed the module from the cryostat and again measured the transmission spectrum at room temperature. The transmission spectrum of the module after cooling are also shown in Fig. 3(b). There was no distinct difference in transmittance before and after cooling, which confirms that the module have no damage by thermal cycles.

3.2 SNSPD performance

We measured the system detection efficiency (η) and the dark count rate (DCR) of the fabricated SNSPD module. The light from the continuous-wave laser diode at 1550 nm wavelength was strongly attenuated to have 10^6 photons/sec and entered to a standard single-mode fibre (SSMF) connector embedded in the hermetic seal of the cryostat. In the cryostat, the SSMF was connected to the high-NA fibre through a thermally expanded core (TEC) fibre. The loss of the TEC fibre was about 1.5 dB at low temperature and less than 0.2 dB at room temperature. Then the high-NA fibre was connected to the SNSPD module cooled at 0.38 K using a ^{3}He cryostat.

Figure 4(a) shows the bias current dependence of the system η and DCR. The system η reaches 32% at the bias of 8 μA. This is over ten times larger than without the SSC. Note that the measured value includes the connection loss between the SSMF and the high-NA fibre of around 1.5 dB, the fibre coupling loss of 1.9 dB, and the loss of the 4.3-mm-long Si waveguide on the chip of 1.6 dB. The estimated the on-chip detection efficiency becomes over 90 % by subtracting the optical losses from the input power. These results confirm that the low temperature integration process did not damage to the NbN nanowire. The system DCR has two components: an exponential increase in the high-bias region and a broad peak in the low- to moderate-bias region. It has been revealed that the former component is the intrinsic DCR of an SNSPD, and the latter is the DCR due to the background blackbody radiation at room temperature passing through an optical fibre. The system DCR is 95 Hz at the bias of 8 μA with the system η of 32%. The system DCR could be further reduced by

integrating a cold band pass filter on the Si chip [21,23]. We have measured the performance of the module more than 10 thermal cycles and confirmed that it was unchanged. Figure 4(b) shows the wavelength dependence of the system η at the bias currents from 7.4 to 8.4 μA. The system η were around 30%, and the variation was less than 0.4 dB at all wavelength. The bandwidth of the SSC is much larger than that of a grating coupler. This is also an advantage for many applications, such as spectral multiplexing [24].

We also measured the timing jitter (Δt) of the SNSPD module. For the measurement, we used a femtosecond fibre laser with the repetition rate of 100 MHz and a time interval analyzer [23]. Figure 4(c) shows the bias current dependence of Δt. The Δt monotonically decreases from 130 to 70 ps as the bias current increases. The value of the jitter is slightly

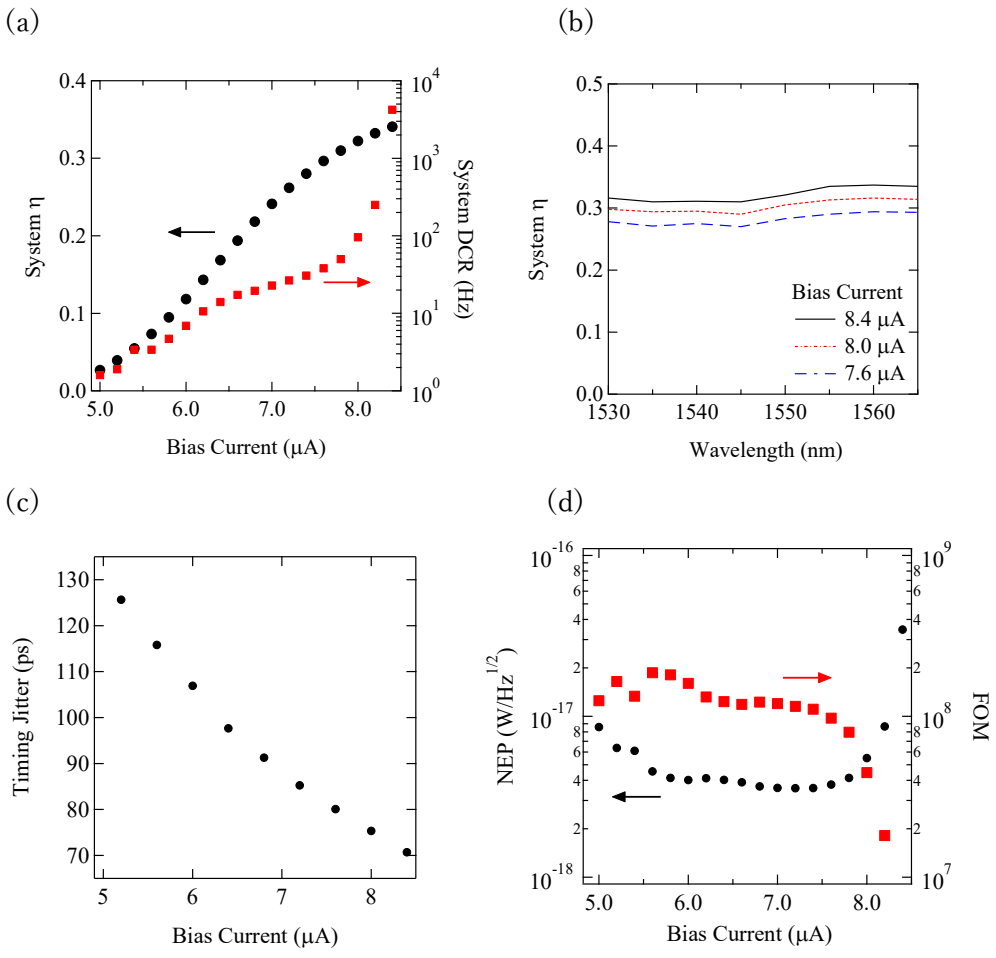

Figure 4. (a) Bias current dependence of system-detection efficiency and dark count rate. (b) Wavelength dependence of system-detection efficiency. (c) Bias current dependence of timing jitter (Δt). (d) Bias current dependence of noise equivalent power (NEP) and the figure of merit (FOM). The temperature is 0.38 K.

larger than that previously reported, which is due to the small bias current of the present module.

To characterize the performance of an ultrasensitive detector, the noise equivalent power (NEP) and/or the figure of merit (FOM) are commonly used. For a single-photon detector, NEP is expressed as NEP = $h\nu(2DCR)^{1/2}/\eta$, where $h\nu$ is the photon energy, and the FOM is defined as FOM = $\eta/(DCR\Delta t)$ [25,26]. Figure 4(d) shows the bias current dependence of the NEP and FOM calculated using the above formulas. The NEP is almost unchanged in the moderate-bias region, and it becomes 3.6×10^{-18} $WHz^{-1/2}$ at the bias current of 7.2 μA. It increases in the low-bias and high-bias regions due to the low system η and the high system DCR, respectively. The FOM reaches 1.9×10^{8} at the bias current of 5.6 μA. These values are better than the previous reported ones for waveguide-integrated SNSPDs.

4. Discussion

Although the system η of 32% is much higher than in the previous reports of waveguide-integrated SNSPDs, it is still lower than that of the meander-type SNSPD. Here, we discuss the possibility of further increasing the system η using our technology. The present chip has a 4.3-mm-long Si waveguide with the loss of 1.6 dB. If the NbN pattern is fabricated just at the edge of the SSC and the loss of the Si waveguide is eliminated, the system η increases to 46%. Furthermore, if we use a high-NA-fibre-connector in the hermetic seal of the cryostat, the TEC fibre can be set outside the cryostat, and the system η can reach 62%. The value is still lower than that of a state-of-the-art meander-type SNSPD, but is large enough to apply to most of the standard integrated quantum photonics. Note that we cannot expect an improvement of the FOM by increasing the system η. Since the system DCR is dominated by the background blackbody radiation in the moderate-bias region, it is also increased by increasing the system η, and the FOM does not change. To improve the FOM, it is necessary to reduce the background blackbody radiation illuminating the SNSPD. Introducing a cold optical filter is the most effective way to decrease the system DCR and improve the NEP and FOM [21,23,26,27]. The demerit of using a cold optical filter is the insertion loss, which degrades the system η. By integrating a cold optical bandpass filter on the Si chip, it seems possible to reduce the insertion loss.

5. Conclusion

We demonstrated a high system-detection-efficiency SNPSD with an SSC, assembled on a fibre-coupled module. The fabricated module showed fibre coupling loss of 1.9 dB and on-chip system detection efficiency of over 90% with a low dark count rate (95 Hz) and small timing jitter (75 ps). The NEP and FOM reaches 3.6×10^{-18} $WHz^{-1/2}$ and 1.9×10^{8},

respectively.

References

[1] Knill E, Laflamme R and Milburn G J, 2001 Nature 409, 46-52
[2] O'Brien J L, 2007 Science 318, 1567-1570
[3] Zbinden H, Bechmann-Pasquinucci H, Gisin N and Ribordy G, 2003 Appl. Phys. B 67, 743
[4] Lo H K, Curty M and Tamaki K, 2014 Nat. Photonics 8, 595-604
[5] Takesue H, Nam S W, Zhang Q, Hadfield R H, Honjo T, Tamaki K and Yamamoto Y, 2007 Nat. Photonics 1, 343-348
[6] Shibata H, Honjo T and Shimizu K, 2014 Opt. Lett. 39 5078-5081
[7] Sharping J E, Lee K F, Foster M A, Turner A C, Schmidt B S, Lipson M, Gaeta A L and Kumar P, 2006 Opt. Express 14, 12388-12393
[8] Lin Q and Agrawal G P, 2006 Opt. Lett. 31, 3140-3142
[9] Matsuda N, Karkus P, Nishi H, Tsuchizawa T, Munro W J, Takesue H and Yamada K, 2014 Opt. Express 22, 22831-22840
[10] Politi A, Cryan M J, Rarity J G, Yu S and O'Brien J L, 2008 Science 320, 646-649
[11] Sprengers J P, Gaggero A, Sahin D, Jahanmirinejad S, Frucci G, Mattioli F, Leoni R, Beets J, Lermer M, Kamp M, Hofing S, Sanjines R and Fiore A, 2011 Appl. Phys. Lett. 99, 181110
[12] Pernice W H P, Schuck C, Minaeva O, Li M, Goltsman G N, Sergienko A V and Tang H X, 2012 Nat. Communications 3, 1325
[13] Najafi F, Mower J, Harris N C, Bellei F, Dane A A, Lee C, Hu X, Kharel P, Marsili F, Assefa S, Berggren K K and Englund D, 2015 Nat. communications 6, 5873
[14] Kahl O, Ferrai S, Kovalyuk V, Goltsman G N, Korneev A and Pernice W H P,2015 Scientific Report 5, 10941
[15] Schuck C, Guo X, Fan L, Ma X, Poot M and Tang H X, 2015 Nat. Communications 7, 10352
[16] Taillaert D, van Laere F, Ayre M, Bogaaerts W, van Thourhout D, Bienstman P and Baets R, 2006 Jpn. J. Appl. Phys. 45, 6071-6077
[17] Shoji T, Tsuchizawa T, Watanabe T, Fukuda H, Yamada K and Morita H, 2002 Electron. Lett. 38, 1669-1670
[18] Tsuchizawa T, Yamada K, Fukuda H, Watanabe T, Takahashi J, Takahashi M, Shoji T, Tamechika E, Itabashi S and Morita H, 2005 IEEE J. Select. Topics Quant. Electron. 11, 232-240
[19] Hiraki T, Nishi H, Tsuchizawa T, Kou R, Fukuda H, Takeda K, Ishikawa Y, Wada K and

Yamada K, 2013 Photon. J. 5, 4500407
[20] Hiraki T, Tsuchizawa T, Yamamoto T, Shibata H and Matsuo S, 2016 in Frontiers in Optics FW5F.3
[21] Shibata H, Shimizu K, Takesue H and Tokura Y, 2013 Appl. Phys. Express 6, 072801
[22] Hiraki T, Tsuchizawa T, Shibata H, Nishi H, Fukuda H, Kou R, Takeda K and Yamada K, 2013 in Proc. of CLEO, CW1O.3
[23] Shibata H, Shimizu K, Takesue H and Tokura Y, 2015 Opt. Lett. 40, 3428-3431
[24] Kahl O, Ferrari S, Kovalyuk V, Vetter A, Malandrakis G L, Nebel C, Korneev A, Goltsman G and Pernice W, 2017 Optica 4, 557-562
[25] Hadfield R H, 2009 Nat. Photonics 3, 696-705
[26] Shibata H, Fukao K, Kirigane N, Karimoto S and Yamamoto H, 2017 IEEE Trans. Appl. Supercond. 27, 2200504
[27] Zhang W J, Yang X Y, Li H, You L X, Lv C L, Zhang L, Zhang C J, Liu X Y, Wang Z and Xie X M, 2018 Supercond. Sci. Technol. 31 035012